Materials Today: Proceedings xxx (xxxx) xxx

Contents lists available at ScienceDirect

Materials Today: Proceedings

journal homepage: www.elsevier.com/locate/matpr

3D meso-macroporous carbon derived spruce leaf biomass for excellent electrochemical symmetrical supercapacitor

Erman Taer [a,*], Sukmawati [a], Apriwandi Apriwandi [a], Rika Taslim [b]

[a] Department of Physics, Faculty of Mathematics and Natural Sciences, University of Riau, Pekanbaru 28293, Indonesia
[b] Department of Industrial Engineering, Islamic State University Sultan Syarif Kasim Riau, Pekanbaru 28293, Indonesia

ARTICLE INFO

Article history:
Available online xxxx

Keywords:
Biomass
Carbon
Electrode material
Spruce leaf
Supercapacitor

ABSTRACT

In this study, an EDLC type supercapacitor device followed by extra pseudo-capacitance properties has been synthesized by using spruce leaf waste as 3D-porous carbon source. Consistently, we investigated the effect of chemically activating $ZnCl_2$ at 0.1, 0.3, and 0.5 M on electrochemical and material properties. Through optimized porous carbon, their surface morphology is highly porous rich in 3D followed by high amorphousness. Furthermore, the 0.3 M $ZnCl_2$ impregnated porous carbon elicited a faradaic redox reaction of self-doping heteroatoms that could increase the electrochemical capacitance. Through symmetric-system, the highest specific capacitance reaches 187 Fg^{-1} at 1 Ag^{-1} in 1 M H_2SO_4 electrolyte.

1. Introduction

Nowadays, a lot of research is focused on developing energy conversion systems and optimizing sustainable and environmentally benign energy storage systems due to the continuing crisis of fossil energy sources which have an impact on the world economy, industry, and ecology. DSSC third-generation solar cells, rechargeable batteries, and electrochemical supercapacitors are considered suitable options to meet the increasing energy transfer demands in optimizing energy storage devices and renewable energy conversion systems. Electrochemical supercapacitors are considered ideal targets for future renewable energy storage devices due to their long lifetime, high discharge rate, and excellent power density [1,2]. Furthermore, the main concern is that the energy density is much lower than that of batteries, which is a recent challenge in the latest electrochemical supercapacitor devices. Therefore, great interest has been evident in the exposure to novel porous systems with high accessibility and high energy density along with long-term stability for new-generation supercapacitors. In the last decade, it has been significantly confirmed that carbon-based biomass provides a very large surface area, porous surface morphology, and 2D nanostructures that increase manifold energy density, excellent stability, and high accessibility [3,4].

After nearly half a decade of intensive studies, many researchers have claimed, the high specific surface area (SSA) is not the main key to enhancing the energy density of supercapacitors. High SSA indeed promises abundant active sites that allow ion diffusion at the rich electrode/electrolyte interface. This behavior drastically increases the high specific capacitance as a figure-of-merit for measuring the improved energy density performance of supercapacitors. However, the specific surface area dominated by micropores that have a narrow diameter (<2 nm) limits the ion transport pathways thereby reducing the power density and degrading the work efficiency and life cycle of the supercapacitor device. On the other hand, the behavior of various pore size distributions and 3D hierarchically connected micro-meso-macropores is believed to be a solution to this problem. Their adjustable combination with suitable ratios reveals increased supercapacitor energy density without limiting their high power density performance. Interestingly to discuss, recent work has revealed that increasing the energy density while maintaining high power density can be achieved through the contribution of 3D hierarchical pore structures including micro-meso-macropores combinations which improve the accessibility of ionic charges and wettability of the base materials as doped heteroatoms supporting [5,6]. Recently, a report by Zheng *et al.* 2021 has been performed on carbon materials derived from the kapok flowers with a hierarchical porous structure rich in micropores and mesopores and distinctly oxygen-rich doping as electrode material for EDLC supercapacitor

* Corresponding author.
E-mail address: erman.taer@lecturer.unri.ac.id (E. Taer).

https://doi.org/10.1016/j.matpr.2023.01.371

[7]. These carbon-based materials can be efficiently synthesized from the raw materials via the procedure route carbonization and activation of KOH at 700 °C. Surprisingly, this study shows high EDLC properties followed by apparent capacitance behavior. In another study, Okonkwo *et al.* 2020 studied nitrogen-rich porous carbon obtained from Spirulina-mediated castor shells via KOH impregnation [8]. This study demonstrated that the specific capacitance could be increased by 365 F g^{-1} in a three-electrode system with a maximum energy density of 9.14 F g^{-1}. Multi-doped heteroatom combinations have also been described in detail by Luo *et al.* 2021 [9] and Wang *et al.* 2022 [10] with various biomass-derived products. In addition, similar results were also confirmed in different waste biomass such as garlic peel [11], sakura flower [12], and banana leaves [13]. On the other hand, $ZnCl_2$ activation is believed to be very suitable and suitable for the design of biomass-based binder-free solid carbon, as reported by Taer *et al* [14,15]. As an example, activated carbon from leek waste which is designed to resemble solid coins through activation of KOH, NaOH, and $ZnCl_2$ shows the best pore and electrochemical properties in the $ZnCl_2$ activating agent with a specific capacitance of 170.12 F g^{-1}. In addition, the 3D hierarchical pore carbon that has been obtained from *Moringa oleifera* leaves is also synthesized through the activating agent $ZnCl_2$. In the solid carbon design, their capacitance is increased by 257 F g^{-1} in a two-electrode system. However, it is very rare to find a biomass precursor that has the potential of a 3D hierarchical pore structure and is doped with heteroatoms at the same time. Additionally, the difficulty of routing large amounts of synthesis at minimal cost prevented it from being widely developed.

On the other hand, spruce leaves are a potential biomass as a carbon source with a regular pore structure. This indication is assumed to originate from the basic appearance of the dark green leaves which have 41 % cellulose and 35.1 % lignin as a high carbon source. In addition, to our knowledge, there has been no previous research examining the carbon source of pine needles for electrode materials. Therefore, this is the first study to study the potential of pine leaves as a carbon source for sustainable supercapacitor applications.

In this study, we have prepared hierarchically interconnected 3D micro-mesoporous carbons with high porosity and oxygen functional groups as self-doping heteroatoms for supercapacitor applications. The precursor was selected from a new spruce leaf biomass source which was converted into porous carbon with a new approach, environmentally friendly, free of toxic and corrosive compounds through $ZnCl_2$ activation, carbonization, and CO_2 activation. The $ZnCl_2$ activating agent was chosen to optimize the performance of the electrode with a binder-free solid design. Furthermore, the electrode material is designed in a non-bonding solid form which can significantly maintain the high conductivity of the material. The optimized porous carbon exhibits a hierarchically connected 3D pore morphology structure with well-confirmed wettability of the oxygen functional groups. In addition, the electrochemical properties studied in the symmetrical configuration possessed high specific capacitance with a coulombic efficiency of up to 89 %. Therefore, the proposed approach of sourcing the new material from pine leaves enables the synthesis of high-quality carbon as a sustainable electrode material for future supercapacitor applications.

2. Materials and methods

2.1. Materials

Zinc chloride and hydrochloric acid were acquired from Sigma Aldric, Singapore. DI waters are acquired clinically on a lab scale at the same time as sulphuric acid is provided from Panreac Quimica sau. The spruce leaves were received from gardeners who tidied up the lawn at the college of mathematical and natural Sciences, riau university.

2.2. Synthesis of porous carbon from spruce leaves

Spruce leaves are separated from the branches and dried in the sunlight until they turn pale green. Further drying performed with ovendried in 50–250 °C. The route of conversion of dried spruce leaf biomass into powder was conducted through a series of pre-carbonization, crushing of samples using a milling tool, and homogenization using a 250 mesh sieve, as previously reported [16,17]. The dried spruce leaf powders were immersed with zinc chloride solution in various molarities. This study focused on the activating agent concentration of 0.5, 0.3 and 0.1 M. Zinc chloride solutions were synthesized by a commonly reported technique [15,18]. Prepare $ZnCl_2$ in powder form with a mass equivalent to the desired molarity (use the stoichiometric equation). After that, the powder was put into a beaker containing 30 mL of DI water. The mixture was stirred at 300 rpm for 60 min. Subsequently, prepare 30 g of precursor powder and put it into the activating agent solution that has been obtained. Sample powder was mixed with an activating agent and then stirred at a speed of 300 rpm at 80 °C for 120 min. Subsequently, the mixed sample was precipitated and dried to obtain an activated powder with an activating agent in a particle scale of < 60 μm. Furthermore, the dry powder that has been obtained is pressed using a hydraulic press with a metric pressure of 8 tons to obtain a solid coin-like sample with dimensions of 2 cm diameter, 0.2 cm height, and 0.7g mass for the record solid coins obtained free of any binding material. The solid coin sample is put into a horizontally furnace which is integrated with N_2 and CO_2 gases. In this instrument furnace, two stages of pyrolysis are applied including carbonization followed CO_2 activation. Carbonization is performed by flowing N_2 gas from room temperature to a temperature of 289 °C at a heating rate of 1 °C/min, then this process is held for 60 min, after that it is continued to a temperature of 600 °C at a temperature rate of 3 °C/min. Furthermore, the physical activation was carried out from a temperature of 600 °C to 850 °C at a temperature rate of 10 °C/min by passing CO_2 gas. When the furnace temperature reaches the maximum, the physical activation process is held for 150 min. The cooling down process is carried out normally without setting the temperature drop. The porous carbon sample that has been obtained was neutralized using 500 cm^3 DI water.

2.3. Characterization of material properties

The spruce leaf-based porous carbon that has been obtained was evaluated in detail including changes in densities of solid samples, confirmation of wettability, microcrystalline properties, surface morphology, and elemental status. Changes in the density of solid samples were recorded according to reduction of diameter, thickness, and, mass precursors. The sample density was evaluated through the standard equation, as is commonly reported [19,20]. The microcrystalline properties were revealed using the X-ray diffraction (XRD) method at an angle range of 2θ 10°-60° with Cu as anode in step size and step scan time of 0.0260 and 7.1400. Their parameters XRD such as d_{002}/d_{100} and L_c-L_a were also evaluated with Debyee Scherrer equation and Braggs law [21,22]. The functional group was detected using Fourier transform infra-red approach in scan rate and accumulations of 10 min/128. The morphological structure of the porous carbon surface was reviewed by scanning electron microscopy (SEM) at 5000x and 40000x magnifications in 15 kV acceleration voltage. The elemental status of the sample was confirmed using energy dispersive spectroscopy (EDS) at 1000x magnification with an energy range of 0 to 20 KeV.

2.4. Electrochemical measurements

The electrochemical behaviours of spruce leaf biomass-based porous carbon electrodes were evaluated in detail through cyclic voltammetry (CV) and galvanostatic charge–discharge (GCD) techniques in a symmetric supercapacitor cell system in an aqueous electrolyte of 1 M H_2SO_4. The separator electrode was selected from an organic permeable membrane from duck eggshell. The mass effective electrode was prepared in a mass of 21 mg at a diameter of 0.8 cm. CV was measured at a potential voltage of 0 V to 1.0 V with scaning rate of 1–10 mV s^{-1}. The capacitance of the electrodes was calculated using the standard equation, as previously reported. Furthermore, GCD was evaluated at a 0–1 V in 1-10A g^{-1}. Specific capacitance, energy density, power density, and electrode resistance were confirmed in detail through GCD measurements using standard formulas, as previously reported studies [23].

3. Results and discussions

The analysis of monolithic solid dimensional changes of spruce-based porous carbon was evaluated through their density differences in initial and final furnace pyrolysis process, as shown in Fig. 1. The selected straategies routes simultaneously removed the organic compounds of the based material and initiated high biochar [24]. In addition, the chemical reaction of the carbon and the activating agent allows the dehydration of the lignocellulosic complex compounds through their reactions on the carbon chains formed in these components and their breakdown into a porous carbon skeleton. This combination of synthesis routes significantly reduces the porous carbon dimensions as shown in Fig. 1. In initial pyrolysis, the carbon density ranged from 0.7127 to 0.8255 g cm^{-3} at a mean standard deviation of 0.035. The N_2 carbonization from 30 °C to 600 °C allows maximum evaporation of water content and volatiles and decomposes the lignin and hemicellulose chains that bind cellulose [25]. This process allows for high carbon fixed and low ash.

Furthermore, the chemical reaction of the activating agent at temperatures above 500 °C allows significant removal of lignin and cellulose thereby initiating the formation of pores on the carbon walls and optimization of the 2D nanofiber structure [26]. This analysis is more clearly reviewed through SEM micrographs. Furthermore, physical activation through CO_2 gas at a high temperature of 850 °C causes optimal ash evaporation and strengthens the pore walls in the carbon-based material [27]. Of course, these routes significantly reduce the density of porous carbon. In finally pyrolysis, the porous carbon density was reduced to 32 % at an error measurement of 0.045 with a range of 0.5118, 0.5400, and 0.6125 g cm^{-3} for SCL1, SCL3, and SCL5, respectively. SCL3 confirmed the decrease in high density due to the combination of carbonization, chemical activation of 0.3 M, and physical activation of CO_2 allowing the most optimal organic compound evaporation followed by the formation of a high pore structure. Carbon electrodes need this property to improve the work performance of supercapacitor [28].

The phase change behavior and micro-crystallinity of the spruce leaves-based porous carbon were revealed by X-ray diffraction analysis. The XRD pattern obtained shows (see Fig. 2) that the two broad peaks at 2θ angles around 24° and 44° are remarked with the 002 and 100 scattering planes illustrating that the carbon material obtained has turbostratic properties, weak crystallinity, low graphitization, and high amorphous [29,30]. This accounts for the presence of various pores including micropores and abundant mesopores on the surface of carbonaceous materials. Significantly these properties are required to form a rich electrical double layer and high ion accessibility in supercapacitor devices. Furthermore, a weak sharp peak was also confirmed in the XRD pattern indicating the presence of a $CaO/CaCO_3$ impurity with a weak crystalline structure on the carbon material. The $CaO/CaCO_3$ compounds were found in carbonaceous materials at angles 28.3°, 30.7°, 31.9°, and 43.1° which were in agreement with previous studies. The presence of $CaO/CaCO_3$ is contributed by organic compounds from spruce leaf biomass which is rich in Ca elements [20,31]. This analysis is consistent with the EDS analysis discussed in Fig. 5. Table 1 recorded the 2θ angle in the 002 and 100 planes, the XRD parameters of d_{002}/d_{100}, and L_c-L_a. The porous carbon obtained from increasing the concentration of the activating agent from 0.1 M to 0.3 M showed a shift in the scattering angle 002 from 24 to 23 indicating the disturbed pore structure was dominated by micropores [32]. Meanwhile, increasing the concentration higher up to 0.5 M indicates that their angle shifts towards a larger confirming the widening of the pores towards abundant macropores. This is due to the high pore wall erosion at a higher concentration of activator. A similar analysis was also confirmed via SEM micrographs, as shown in Fig. 4.

Furthermore, the d_{002} obtained in the SLCs had a higher value than the d_{002} graphite by about 6–11 %, revealing that the porous carbon exhibited a good amorphous structure [21]. Moreover, the porous carbon SLCs exhibits a relatively low microcrystalline L_c

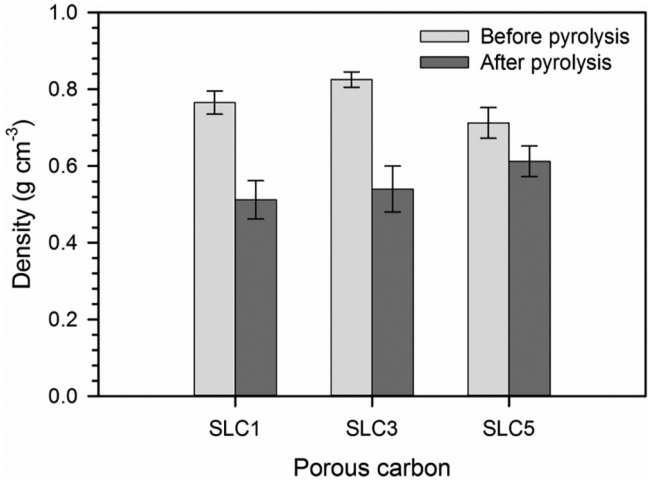

Fig. 1. Porous carbon density at initial-final pyrolysis process.

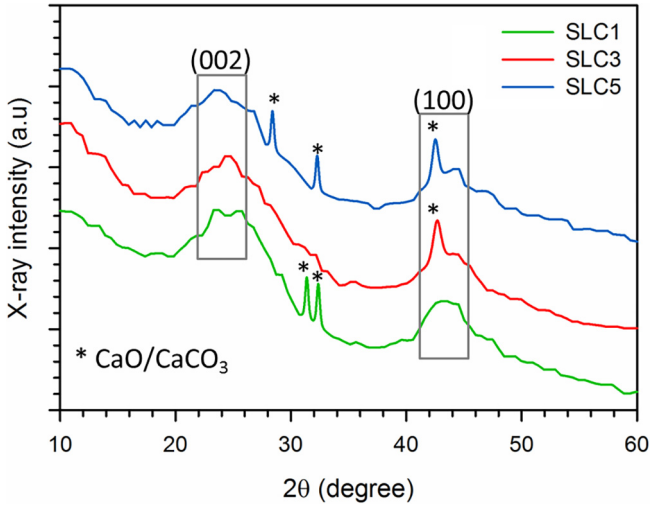

Fig. 2. XRD pattern of spruce leaves-based porous carbon.

Table 1
The XRD parameters of d_{002}/d_{100} and L_c-L_a.

Porous carbon	$2\theta_{002}$ (°)	$2\theta_{100}$ (°)	d_{002} (nm)	d_{100} (nm)	L_c (nm)	L_a (nm)
SLC1	24.479	44.053	0.3575	0.2053	0.8120	41.138
SLC3	23.676	44.498	0.3754	0.2034	0.7563	36.653
SLC5	24.924	44.868	0.3569	0.2018	1.0056	21.820

dimension indicating a relatively high surface area as an ideal active site for electrolyte ions. The specific surface area of the porous carbon can be predicted using L_c through an empirical approach, as previously reported [22,33]. The L_c parameter is inversely related to the specific surface area prediction as their empirical formula $SSA_{xrd} = 2/\rho L_c$. According on these empirical equations, SLC3 displays largest surface area of about 1120 $m^2\ g^{-1}$.

SLCs surface functional groups were recorded by the FTIR approach. Fig. 3 illustrated the FTIR spectra of the spruce-leaves porous carbon SLC3 and SLC5. It can be seen clearly that the absorbance peaks were relatively complex at the wavelength of 4500–500 cm^{-1}. The SLC3 sample illustrated an absorption peak at 3469 cm^{-1} related to the –OH hydroxy functional group in strain mode due to the adsorption of water content [34]. The C—H strain band is observed faintly at 2953 cm^{-1} [35].

Furthermore, the absorption peaks at 2570 and 1648 cm^{-1} were indicated for the C—H/C═O carboxylic acids and phenol [36]. The wavenumber of 1410 cm^{-1} is described to the C═C bond followed by a stretch band along 1226 cm^{-1} to 653 cm^{-1} which is closely related to the C—O bond originating from the alcohol, phenol, and carboxylic acid strains [37]. The chemical impregnation route using $ZnCl_2$ at a concentration of 0.3 M significantly displayed oxygen-rich functional groups. This characteristic significantly contributes to increasing the wettability of the sample surface which initiates the presence of redox behavior in electrodes material. This characteristic is frequently encountered in the literature as a heteroatom self-doping effect, as previously reported [38,39].

Moreover, the impregnation of $ZnCl_2$ at a higher concentration of up to 0.5 M in SLC5 indicated a shift in the –OH strain band to 3458 cm^{-1} confirming the formation of more oxide compounds. In addition, the deformation of phenol and carboxylic acids along wave number 2905 to 1889 cm^{-1} indicates high dehydration of the porous carbon. In addition, the C—O strain band at 1639 cm^{-1} was confirmed to be higher than SLC3 indicating high oxygen in SLC5. Meanwhile, alcohol, phenol, and carboxylic acid along the absorption band 1236–654 cm^{-1} were reduced faintly revealing the evaporation of water content and elemental oxygen in the porous carbon sample. However, some oxygen functional groups are significantly associated with carbon and hydrogen in the prepared samples initiating enhanced heteroatom self-doping properties for the material electrodes [18,40]. This analysis was confirmed in detail through the elemental status confirmation and performance of the EDLC devise through the EDS and CV-GCD techniques.

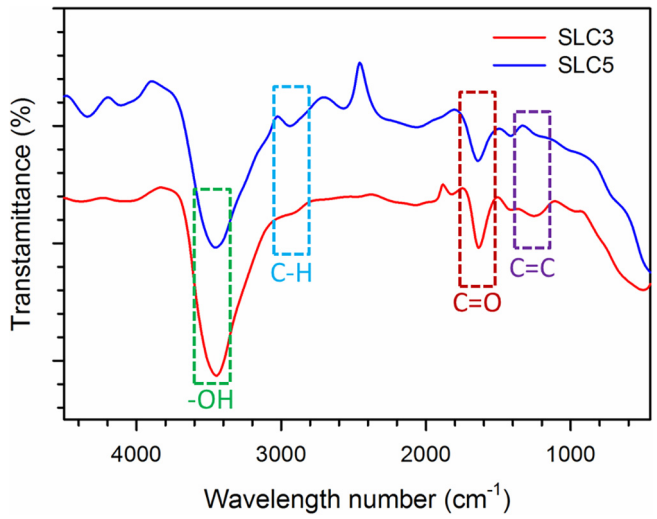

Fig. 3. FTIR spectra of spruce leaves-based porous carbon.

The surface morphology structure of spruce leaves-based porous carbon was reviewed by scanning electron microscopy (SEM) at 5000x and 4000x mags, as shown in Fig. 4. The selected porous carbon synthesis route included $ZnCl_2$ impregnation at different solution concentrations, N_2 carbonization, and CO_2 physical activation has markedly displayed an abundance of diverse framework and it also 2D nanofiber nanostructures. As shown in Fig. 4a, SEM micrographs of SLC3 display particle and block carbon aggregates in the size range of 0.26 μm to 4.28 μm. In addition, they also surprisingly illustrate 3D pore structures at varying sizes in macro to micro scales. At 4000x magnification area, SLC3 confirmed their potential in presenting various hexagonal pores resembling a honeycomb which on the side walls are decorated with narrow interconnected pores, as shown in Fig. 4b. This revealed that the SLC3 sample had 3D hierarchical pores including micro, meso, and macropores which contributed greatly to the enhanced specific capacitance of EDLC type of supercapacitor [41]. Micropores that are on a small scale of 2 nm contribute to providing a high active site corresponding to the charge of the electrolyte ion to form a high electrical layer thereby increasing the energy density of the supercapacitor [42].

Furthermore, the combination of mesopores in the range of 2–50 nm and macropores larger than 50 nm enables carbon electrodes to have high ion accessibility, very fast charge transfer, ion buffering, and ion diffusion capability in all directions which initiates their high power density [43]. Therefore, the combination of these three pore scales drastically increases the specific capacitive of the supercapacitor energy storage device. This analysis is strongly supported by the CV and GCD analyses discussed in Fig. 6 and Fig. 7.

Moreover, the impregnation of $ZnCl_2$ at the highest concentration in SLC5 surprisingly changed the surface structure of the precursor. Particle aggregates and carbon blocks were found to be relatively small in size, as confirmed on the 5000x magnification SEM micrograph in Fig. 4c. Their 3D pore structure is reduced due to high chemical impregnation which dehydrates too much carbon thereby eroding the pore walls and causing the pore framework to collapse. Interestingly, excessive etching of carbon chains at a concentration of 0.5 M allowed obtaining nanofiber structures on their surfaces, as shown in Fig. 4d. SEM SLC5 micrograph at 4000x magnification noticeably revealed 2D nanofiber nanostructures at 98 nm diameter. This allows relatively small pores to adhere along the nanofiber surface. In addition, this nanofiber structure initiates high conductivity for the material's electrodes [44]. In comparison, the morphological structure of spruce leaves carbon has similarities with previous studies such as garlic peel, etc.

The elemental status of the spruce leaves precursors converted into porous carbon through multi-activation of $ZnCl_2$-CO_2 was revealed by energy dispersive spectroscopy (EDS) technique in

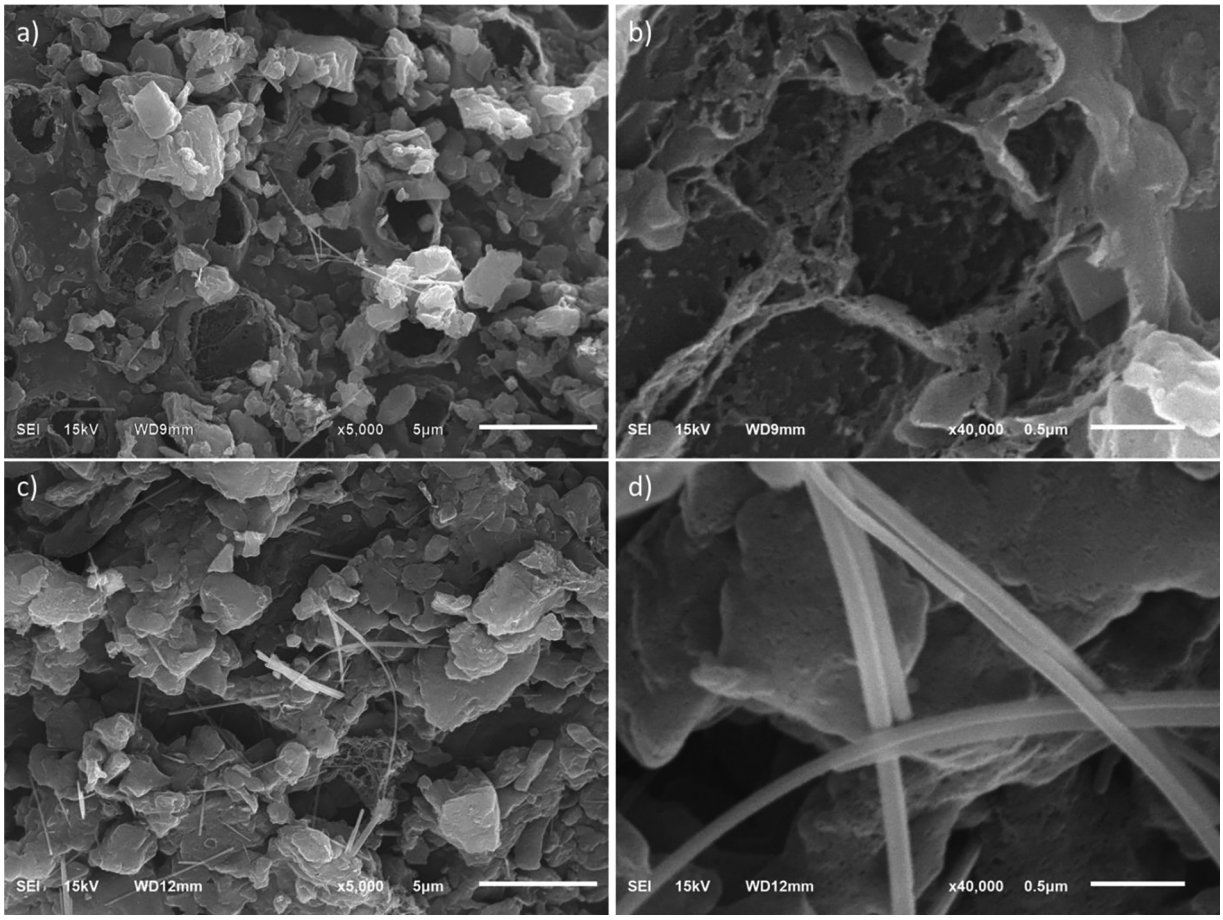

Fig. 4. Micrograph SEM of a) SLC3 in 5000x magnification, b) SLC3 in 40000x magnification, c) SLC5 in 5000x magnification, and d) SLC5 in 40000x magnification.

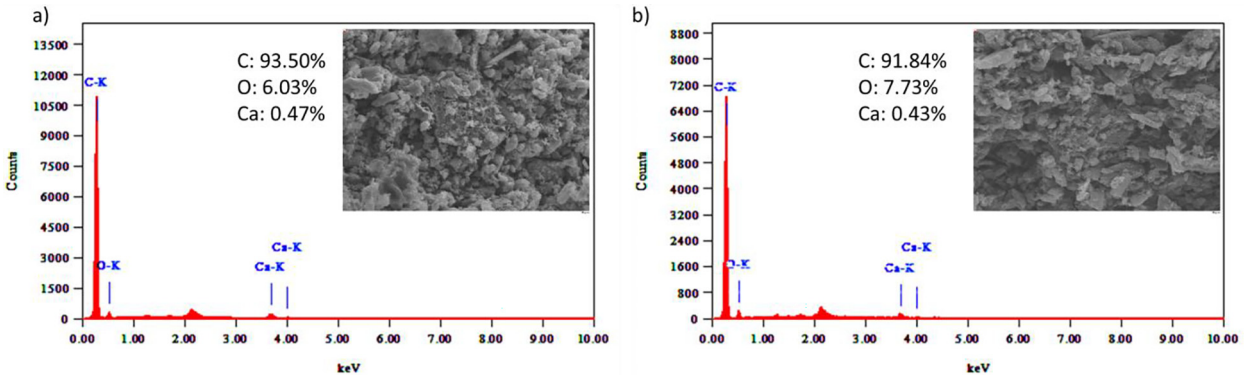

Fig. 5. EDS spectra of a) SLC3, and b) SLC5 samples.

the energy range of 0–20 keV. In general, the selected synthesis route has succeeded in obtaining biochar samples with high carbon quality at 91–93 %, as shown in Fig. 5. Furthermore, elemental oxygen occupies the highest elemental status after carbon indicates that oxide compounds are still present in the sample, in lower concentrations. In addition, the relatively high presence of oxygen confirms the previously discussed XRD and FTIR analysis that the sample significantly exhibits wettability in the sample acting as a doped self-heteroatom [18,45]. Additionally, elemental calcium was confirmed to be very low in the sample as a result of incompletely evaporated organic precursor compounds revealing the presence of $CaO/CaCO_3$ compounds as confirmed by XRD.

Fig. 5a displays the EDS spectra with the highest carbon, revealing that the SLC3 sample has high purity properties followed by an oxygen content of 6.035 %. Increasing the concentration of $ZnCl_2$ at a higher concentration reduces the organic precursor elements to 0.43 %, as shown in Fig. 5b. However, the dehydrating agent $ZnCl_2$ causes an excessive oxidation reaction thereby reducing the carbon content to 91.03 % and increasing elemental oxygen to 7.73 %. However, the overall carbon yield is relatively high which can improve the quality of the electrode material as an electrochemical energy storage device.

The electrochemical properties of spruce leaves-based biochar pyrolyzed at high temperature and chemical impregnation of zinc

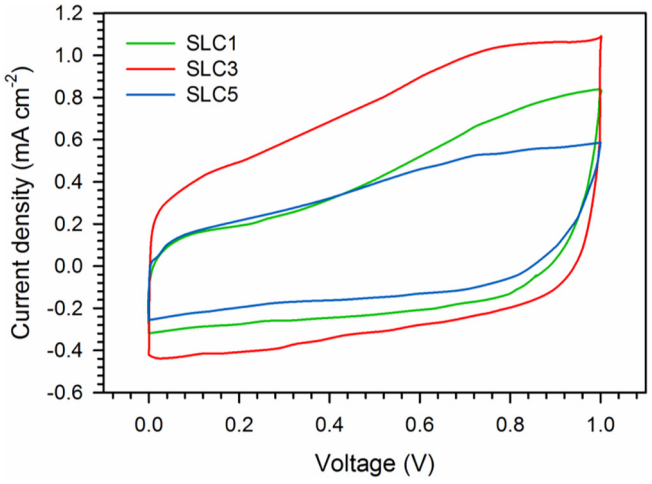

Fig. 6. CV profile of SLC1, SLC3, and SLC5.

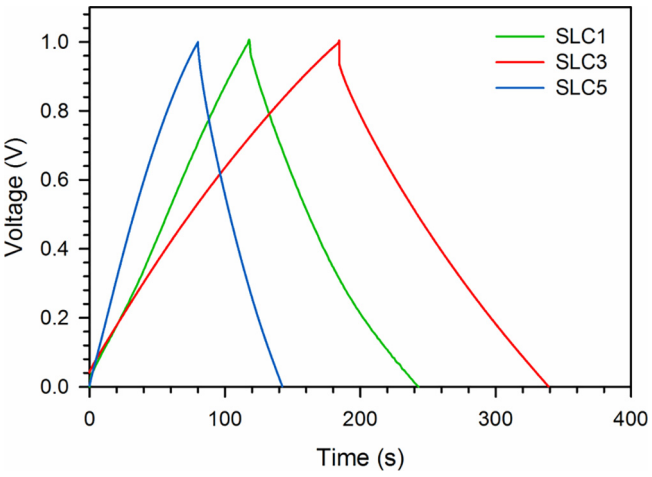

Fig. 7. The GCD profile of SLC1, SLC3, and SLC5.

chloride at different solution concentrations in the range of 0.1, 0.3, and 0.5 M were evaluated through cyclic voltammetry and galvanostatic charge–discharge techniques in aqueous electrolyte H_2SO_4. The working electrodes are assembled in a symmetric supercapacitor system consisting of two solid carbon-based spruce leaves (average working mass of 21 mg), a separator from an organic semipermeable membrane, a current collector made of stainless steel, and an aqueous electrolyte of 1 M H_2SO_4. The CV analysis was reviewed in the standard voltage range from 0 V to 1.0 V at a scan rate of 1 mV s^{-1}. Next, the specific capacitance is calculated by means of the charge and discharge currents listed in the CV test, according to the standard formula. The CV profile of the spruce leaf-based porous carbon is illustrated in Fig. 6, showing that the SLC1, SLC3, and SLC5 electrodes reveal a distorted rectangular hysteresis curve shape characterizing the normal electrical double layer state [46].

Furthermore, the increase in density that forms a wide hump in the voltage range of 0.62 < U < 0.82 confirms the extra pseudocapacitance of the redox reaction that occurs as a contribution from the self-doping of oxygen heteroatoms. In addition, the CV profile confirms the capacitive nature of the electrode where a large hysteresis area indicates a high specific capacitance and vice versa. In detail, the SLC1 electrode exhibits a CV profile displaying a sizeable CV profile confirming a specific capacitance of 104 F g^{-1}. In addition, at U > 0.52, a significant increase in current density was found, describing the redox reaction of the oxygen functional group which gave more ionic charge to the device system. This clearly indicates the presence of pseudo-capacitance at the electrode.

Furthermore, the CV profile of the SLC3 electrode shows the largest rectangular shape followed by a wide current density hump at 0.62 < U < 0.82 indicating the outstanding capacitive properties and obvious pseudo-capacitance properties. Their specific capacitance is the highest at 141 F g^{-1} compared to other electrodes. The amazing combination of material properties of SLC3 carbon including amorphous, high porosity, predicted largest specific surface area, 3D hierarchical pore structure, wettability, and self-oxygen doped dramatically enhances the high performance of the electrodes resulting in maximum optimized energy storage devices [47,48].

Moreover, the SLC5 electrode displayed the smallest CV profile of the three test electrodes, revealing a low specific capacitance of 75 F g^{-1}. This confirms that the reduction of the 3D pore frame structure drastically reduces the electrode capacitive properties of the material, as shown in the SEM micrograph Fig. 4c. In addition, the effect of the redox reaction of the oxygen functional group is getting weaker and looks faint indicating reduced pseudo-capacitance. This certainly has an effect on the weakening of the capacitive properties of the SLC5 electrode.

The electrochemical properties of symmetrical cell supercapacitors SLC1, SLC3, and SLC5 were further investigated by galvanostatic charge–discharge (GCD) at a current density of 1 A g^{-1} in a scan rate of 1 mV s^{-1}, as shown in Fig. 7. The GCD profile displays an almost ideal isosceles triangular shape showing the high potential of the electrode to produce normal electrical double layer capacitive behavior. In addition, the very small voltage drop (iR drop) in the initial discharge stage characterizes the relatively weak electrode resistance in aqueous electrolyte. Furthermore, their charge and discharge times reflecting a coulombic efficiency of 70–89 % revealed the presence of a pseudo-capacitance effect in the electrodes of SLCs. In addition, the long charge–discharge time indicates the specific capacitance of the supercapacitor electrodes.

In detail, the SLC1 electrode exhibits a sufficiently long charge–discharge time identifying a specific capacitance of 106 F g^{-1} at an electrode resistance of 0.02 Ω. Chemical activation of $ZnCl_2$ in 0.1 M solution can produce relatively high capacitive properties of some previous studies derived from biomass. Interestingly, increasing the concentration of $ZnCl_2$ solution at 0.3 M drastically increased the specific capacitance of the SLC3 electrode to 187 F g^{-1}. This is due the chemical impregnation of $ZnCl_2$ 0.3 M can significantly present an interconnected 3D pore structure from micro to macropores and followed the high specific surface area of 1120 m^2 g^{-1}. Micro-meso-macropores significantly increase the provision of high active channels at the electrolyte/electrode interface followed by high ion accessibility [49]. Therefore, their capacitive properties are improved by almost 2 times. Furthermore, the wettability property of the oxygen functional group elicits a faradaic redox reaction at the SLC3 electrode initiating extra pseudocapacitance. However, the growth of high narrow pores on the SLC3 electrode significantly inhibited the flow of ionic charge thereby increasing the electrode resistance by 0.43 Ω.

Moreover, the addition of a higher concentration of $ZnCl_2$ solution on chemical activation allows the removal of more pore framework walls thereby reducing their capacitive properties, as shown in the GCD profile for the SLC5 sample. The SLC5 electrode showed the lowest specific capacitance of 30 F g^{-1}. This reduction in capacitive properties is due to an increase in pore volume on a macro scale which significantly reduces the active channel corresponding to the selected electrolyte ion. On the other hand, the SLC5 electrodes showed the lowest electrode resistance of

0.009 Ω indicating that they had the highest ion accessibility compared to the other two electrodes.

As illustrated in Fig. 8, the energy and power specific (Wh kg^{-1} and W kg^{-1}) of the SLCs were confirmed by means of a Ragone plot. The SLC1 electrode displays a relatively low energy density equal to 0.60 Wh kg^{-1} at a power density of 96.60 W kg^{-1}. The increasing concentration of $ZnCl_2$ on the SLC3 electrode showed the highest energy density reaching 8.07 Wh kg^{-1} at an optimum power density of 94.00 W kg^{-1}. This confirms that the presence of 3D pores and oxygen functional groups can increase the high energy density of the EDLC-type supercapacitor electrodes. Meanwhile, the SLC5 electrode has an energy density of 3.25 Wh kg^{-1} at a power density of 98.80 W kg^{-1}.

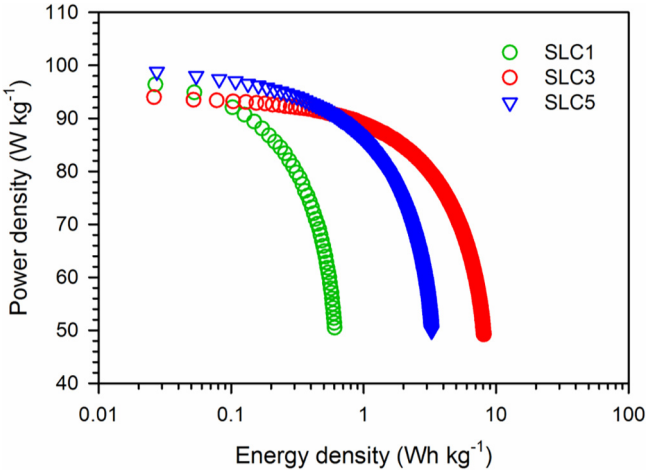

Fig. 8. Ragone plot of SLC1, SLC3, and SLC5.

The best performance of SLC3 was reviewed comprehensively through electrochemical impedance spectroscopy (EIS) technique in symmetrical electrodes separated by a duck eggshell membrane and 1 m/L H_2SO_4 aqueous electrolyte. Based on EIS measurements, Nyquist plot, bode phase plot, bode plot of real capacitance, and bode plot imaginary capacitance were illustrated in Fig. 9a-d. Nyquist plots reveal the capacitive properties of the SLC3 symmetrical electrodes approaching the ideal behavior of electrochemical double layer capacitance with a liquid electrolyte, as confirmed by the markedly increasing impedance pattern in the low-frequency region up to 10 mHz. In the mid-frequency region, a straight line with a slope of about 45° refers to the Warburg resistance, which results from the insertion/de-insertion of ions in the hierarchical pores of the spruce leaves-based electrode material. Furthermore, the semicircular features in the high-frequency region represent the ionic resistance of the electrolyte, the electrode resistance, and the geometric/double layer capacitance values. The ionic resistance of the electrolyte and the bulk resistance of the SLC3 electrode were evaluated from the intersection of the Nyquist plot and the real axis which is often referred to as the series resistance (R_s) of 1.039 Ω cm^{-2}. This relatively low value of R_s indicates high capacitive properties for supercapacitor cells. On the other hand, the charge transfer resistance (Rct) was evaluated from the intersection of the semicircular arcs on the Z axis. The R_{ct} value obtained at 4.071 cm^{-2} is closely related to the Faradaic redox reaction occurring at the electrode–electrolyte

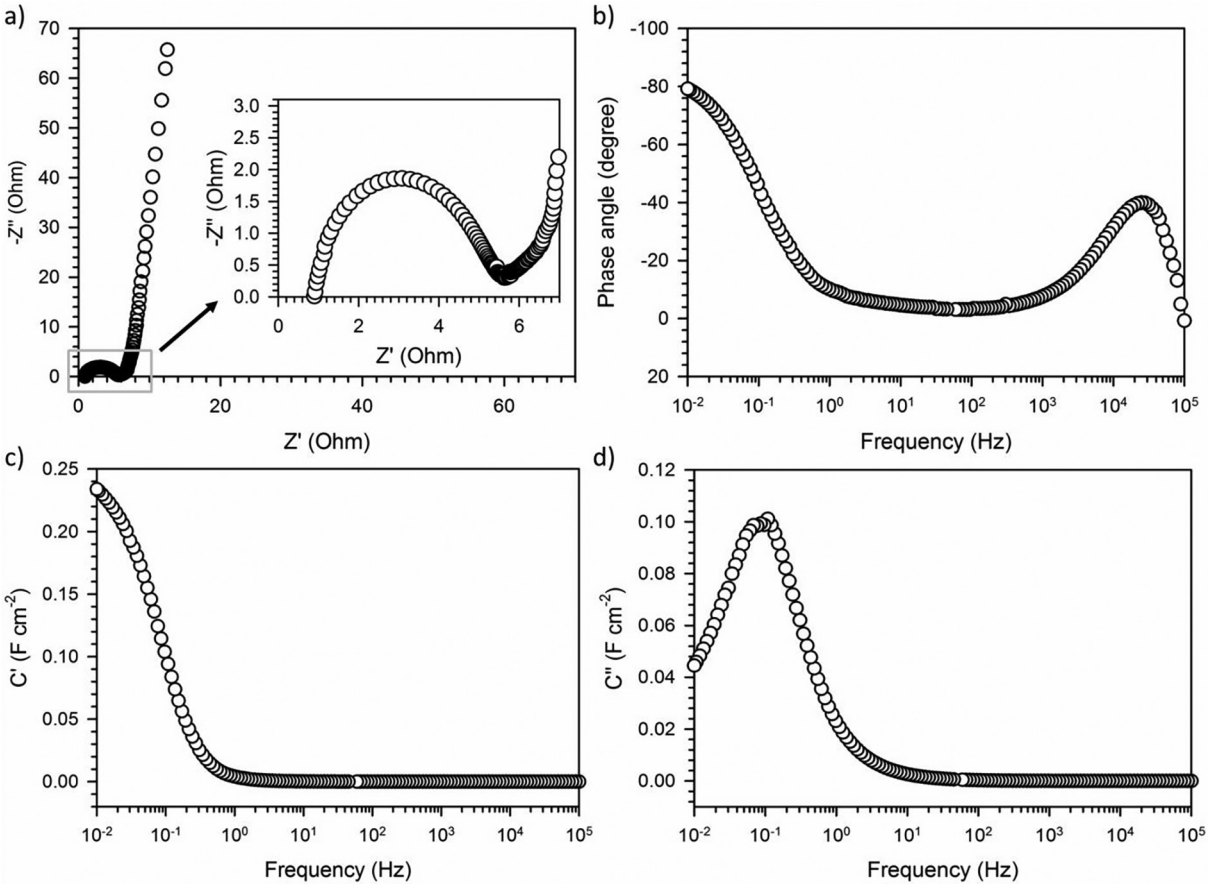

Fig. 9. A) Nyquist plot, b) bode phase plot, c) real capacitance vs frequency curve, and d) imaginer capacitance vs frequency curve.

interface, initiating a pseudocpacitive effect on the SLC3 electrode. This analysis was also clearly confirmed on the CV and GCD measurements which have been discussed in Fig. 6 and Fig. 7. In principle, the charge transfer resistance (R_{ct}) was observed as a result of the OH/COOH functional group attached to the activated carbon surface which was found to be adsorbed on the biomass carbon-based electrodes as shown in FTIR spectrum. This adsorbed functionality is responsible for Faradaic (pseudocapacitive) reactions with electrolyte ions, and the main reason for obtaining R_{ct} values in the electrodes of biomass carbon-based supercapacitors [1–3]. Furthermore, the Bode plot of the phase-to-frequency angle illustrated in Fig. 9b confirms the angle value close to −90° at the minimum frequency. This shows that the SLC3 electrode has an ideal capacitive behavior. In addition, a frequency (f_p) at a phase angle of 45° representing a value of about 0.108 Hz can be applied to determine the lifetime of the ionic charge (τ) of the SLC3 electrode. Through the $1/f_p$ equation, the relatively small ion lifetime reveals the potential of the SLC3 electrode for efficient and stable supercapacitor applications. Moreover, the bode plot on the part of the real and imaginary capacitances is shown in Fig. 9c-d. As reported by many studies [4], C' represents realeliverable capacitance, while C' represents energy loss. SLC3 electrodes show C' values which are highly dependent on low frequencies and lower their value at higher frequencies confirming the purely resistive behavior of supercapacitor cells. In addition, C'' also shows almost similar behavior, but a peak (f_p) is found at low frequencies. The peak frequency (f_p) of about 0.108 Hz can be applied to determine the lifetime of the ionic charge (τ) of the SLC3 electrode. Through equation $1/f_p$, the relatively small ion lifetime reveals the potential of the SLC3 electrode for efficient and stable supercapacitor applications.

4. Conclusions

In conclusion, porous carbon synthesized through a combination of chemical activation and physical activation from spruce leaf derivatives has succeeded in obtaining a 3D pore structure to improve the high performance of the electrode material as electrochemical energy storage. Furthermore, chemical activation of $ZnCl_2$ at different solution concentrations followed by high-temperature physical activation resulted in the wettability of the oxygen functional group. Furthermore, the surface morphology suggests potential precursors provide a 3D carbon skeleton of the meso-macropores combination. As a result, the electrode-based specific capacitance of SLCs has increased rapidly to reach 187 F g^{-1} at a current density of 1 A g^{-1}. In addition, the optimized carbon electrode has excellent stability with a coulombic efficiency of up to 89 %. The highest energy density of porous carbon-based devices from spruce leaves can reach 8.07 Wh kg^{-1}. Therefore, we have generated a 3D structure of carbon derived from spruce leaves waste for potential applications of implantable EDLC-type supercapacitor devices and electronic components in the future.

CRediT authorship contribution statement

Erman Taer: Conceptualization, Methodology. **Sukmawati:** Resources. **Apriwandi Apriwandi:** Formal analysis, Data curation, Writing – original draft, Writing – review & editing. **Rika Taslim:** Visualization, Validation.

Data availability

Data will be made available on request.

Declaration of Competing Interest

The authors declare that they have no known competing financial interests or personal relationships that could have appeared to influence the work reported in this paper.

Acknowledgements

The research was supported by second year Project of Word Class Research (WCR) in *Kementerian pendidikan, Kebudayaan, Riset, dan Teknologi*, Republic of Indonesia with contract No: 1627/UN19.5.1.3/PT.01.03/2022. Project title: "*Superkapasitor dengan Rapat Energi dan Daya Tinggi: Optimalisasi Proses Penyediaan Elektroda*".

References

[1] K. Poonam, A. Sharma, S.K. Arora, Tripathi, Review of supercapacitors: Materials and devices, J. Energy Storage. 21 (2019) 801–825, https://doi.org/10.1016/j.est.2019.01.010.
[2] Z.S. Iro, C. Subramani, S.S. Dash, A brief review on electrode materials for supercapacitor, Int. J. Electrochem. Sci. 11 (2016) 10628–10643. 10.20964/2016.12.50.
[3] A.R. Selvaraj, A. Muthusamy, H.J. In-ho-Cho, K. Kim, K.P. Senthil, Ultrahigh surface area biomass derived 3D hierarchical porous carbon nanosheet electrodes for high energy density supercapacitors, Carbon N.Y. 174 (2021) 463–474, https://doi.org/10.1016/j.carbon.2020.12.052.
[4] E.E. Miller, Y. Hua, F.H. Tezel, Materials for energy storage: Review of electrode materials and methods of increasing capacitance for supercapacitors, J. Energy Storage. 20 (2018) 30–40, https://doi.org/10.1016/j.est.2018.08.009.
[5] Q. Abbas, R. Raza, I. Shabbir, A.G. Olabi, Heteroatom doped high porosity carbon nanomaterials as electrodes for energy storage in electrochemical capacitors: A review, J. Sci. Adv. Mater. Devices. 4 (2019) 341–352, https://doi.org/10.1016/j.jsamd.2019.07.007.
[6] Y. Zhang, S. Yu, G. Lou, Y. Shen, H. Chen, Z. Shen, S. Zhao, J. Zhang, S. Chai, Q. Zou, Review of macroporous materials as electrochemical supercapacitor electrodes, J. Mater. Sci. 52 (2017) 11201–11228, https://doi.org/10.1007/s10853-017-0955-3.
[7] L.H. Zheng, M.H. Chen, S.X. Liang, Q.F. Lü, Oxygen-rich hierarchical porous carbon derived from biomass waste-kapok flower for supercapacitor electrode, Diam. Relat. Mater. 113 (2021), https://doi.org/10.1016/j.diamond.2021.108267.
[8] C.A. Okonkwo, T. Lv, W. Hong, G. Li, J. Huang, J. Deng, L. Jia, M. Wu, H. Liu, M. Guo, The synthesis of micromesoporous carbon derived from nitrogen-rich spirulina extract impregnated castor shell based on biomass self-doping for highly efficient supercapacitor electrodes, J. Alloys Compd. 825 (2020), https://doi.org/10.1016/j.jallcom.2020.154009.
[9] L. Luo, L. Luo, J. Deng, T. Chen, G. Du, M. Fan, W. Zhao, High performance supercapacitor electrodes based on B/N Co-doped biomass porous carbon materials by KOH activation and hydrothermal treatment, Int. J. Hydrogen Energy. 46 (2021) 31927–31937, https://doi.org/10.1016/j.ijhydene.2021.06.211.
[10] J. Wang, Y. Xu, M. Yan, B. Ren, X. Dong, J. Miao, L. Zhang, X. Zhao, Z. Liu, Preparation and application of biomass-based porous carbon with S, N, Zn, and Fe heteroatoms loading for use in supercapacitors, Biomass Bioenergy 156 (2022), https://doi.org/10.1016/j.biombioe.2021.106301.
[11] T. Ji, K. Han, Z. Teng, J. Li, M. Wang, J. Zhang, Synthesis of Activated Carbon Derived from Garlic Peel and Its Electrochemical Properties, Int. J. Electrochem. Sci. 16 (2021) 1–14. 10.20964/2021.01.61.
[12] F. Ma, S. Ding, H. Ren, Y. Liu, Sakura-based activated carbon preparation and its performance in supercapacitor applications, RSC Adv. 9 (2019) 2474–2483, https://doi.org/10.1039/c8ra09685f.
[13] A. Apriwandi, E. Taer, R. Farma, R.N. Setiadi, E. Amiruddin, A facile approach of micro-mesopores structure binder-free coin/monolith solid design activated carbon for electrode supercapacitor, J. Energy Storage. 40 (2021), https://doi.org/10.1016/j.est.2021.102823.
[14] E. Taer, R. Taslim, A. Apriwandi, Ultrahigh capacitive supercapacitor derived from self-oxygen doped biomass-based 3D porous carbon sources, ChemNanoMat 8 (2022) e202100388.
[15] E. Taer, R. Taslim, A. Apriwandi, Biomass-based self-single-oxygen heteroatom doped hierarchical porous carbon nanosheet for high-performance symmetrical supercapacitor, ChemNanoMat 8 (2022) e202200217.
[16] E. Taer, R. Taslim, Brief Review: Preparation Techniques of Biomass Based Activated Carbon Monolith Electrode for Supercapacitor Applications, in: AIP Conf. Proc., 2018, pp. 020004-1–020004-4. https://doi.org/10.1063/1.5021192.
[17] R. Farma, M. Deraman, R. Omar, M.M. Awitdrus, E. Ishak, I.A.T. Taer, Binderless composite electrode monolith from carbon nanotube and biomass carbon activated by KOH and CO2 gas for supercapacitor, AIP Conference Proceedings 1415 (2011) 180–184, https://doi.org/10.1063/1.3667251.
[18] E. Taer, A. Apriwandi, N. Nursyafni, R. Taslim, Averrhoa bilimbi leaves-derived oxygen doped 3D-linked hierarchical porous carbon as high-quality electrode

material for symmetric supercapacitor, J. Energy Storage. 52 (2022), https://doi.org/10.1016/j.est.2022.104911.
[19] E. Taer, K. Natalia, A. Apriwandi, R. Taslim, A. Agustino, R. Farma, The synthesis of activated carbon nano fiber electrode made from acacia leaves (Acacia mangium wild) as supercapacitors, Adv. Nat. Sci. Nanosci. Nanotechnol. 11 (2020) 25007, https://doi.org/10.1088/2043-6254/ab8b60.
[20] E. Taer, Apriwandi, B.K.L. Dalimunthe, R. Taslim, A rod-like mesoporous carbon derived from agro-industrial cassava petiole waste for supercapacitor application, J. Chem. Technol. Biotechnol. 96 (2021) 662–671, https://doi.org/10.1002/jctb.6579.
[21] J. Serafin, M. Baca, M. Biegun, E. Mijowska, R.J. Kaleńczuk, J. Sreńscek-Nazzal, B. Michalkiewicz, Direct conversion of biomass to nanoporous activated biocarbons for high CO2 adsorption and supercapacitor applications, Appl. Surf. Sci. 497 (2019), https://doi.org/10.1016/j.apsusc.2019.143722.
[22] M. Deraman, R. Daik, S. Soltaninejad, N.S.M. Nor, R. Awitdrus, N.F. Farma, N.H. Mamat, M.A.R.O. Basri, A new empirical equation for estimating specific surface area of supercapacitor carbon electrode from X-ray diffraction, Adv. Mater. Res. 1108 (2015) 1–7, https://doi.org/10.4028/www.scientific.net/AMR.1108.1.
[23] R. Vicentini, L.M. Da Silva, E.P. Cecilio, T.A. Alves, W.G. Nunes, H. Zanin, How to measure and calculate equivalent series resistance of electric double-layer capacitors, Molecules 24 (2019), https://doi.org/10.3390/molecules24081452.
[24] E. Taer, N. Yanti, W.S. Mustika, A. Apriwandi, R. Taslim, A. Agustino, Porous activated carbon monolith with nanosheet/nanofiber structure derived from the green stem of cassava for supercapacitor application, Int. J. Energy Res. 44 (2020) 1–14, https://doi.org/10.1002/er.5639.
[25] E. Taer, A. Afrianda, R. Apriwandi, A.A. Taslim, R.F. Awitdrus, Production of activated carbon electrodes from Sago waste and its application for an electrochemical double-layer capacitor, Int. J. Electrochem. Sci. 13 (2018) 10688–10699. 10.20964/2018.11.27.
[26] T.R. Kumar, R.A. Senthil, Z. Pan, J. Pan, Y. Sun, A tubular-like porous carbon derived from waste American poplar fruit as advanced electrode material for high-performance supercapacitor, J. Energy Storage. 32 (2020), https://doi.org/10.1016/j.est.2020.101903.
[27] E. Taer, Y. Susanti, A. Awitdrus, S. Sugianto, R. Taslim, R.N. Setiadi, S. Bahri, A. Agustino, P. Dewi, B. Kurniasih, The effect of CO2 activation temperature on the physical and electrochemical properties of activated carbon monolith from banana stem waste, AIP Conf. Proc. 1927 (2018) 030016-1–030016-5. https://doi.org/10.1063/1.5021209.
[28] E. Taer, A. Apriwandi, R. Taslim, A. Agutino, D.A. Yusra, Conversion Syzygium oleana leaves biomass waste to porous activated carbon nanosheet for boosting supercapacitor performances, J. Mater. Res. Technol. 9 (2020) 13332–13340, https://doi.org/10.1016/j.jmrt.2020.09.049.
[29] B.S. Girgis, Y.M. Temerk, M.M. Gadelrab, I.D. Abdullah, X-ray diffraction patterns of activated carbons prepared under various conditions, Carbon Sci. 8 (2007) 95–100, https://doi.org/10.5714/cl.2007.8.2.095.
[30] F. Márquez-Montesino, N. Torres-Figueredo, A. Lemus-Santana, F. Trejo, Activated Carbon by Potassium Carbonate Activation from Pine Sawdust (Pinus montezumae Lamb.), Chem. Eng. Technol. 43 (2020) 1716–1725, https://doi.org/10.1002/ceat.202000051.
[31] A.M. Abioye, F.N. Ani, Recent development in the production of activated carbon electrodes from agricultural waste biomass for supercapacitors: A review, Renew. Sustain. Energy Rev. 52 (2015) 1282–1293, https://doi.org/10.1016/j.rser.2015.07.129.
[32] D.C. Martínez-Casillas, I. Mascorro-Gutiérrez, C.E. Arreola-Ramos, H.I. Villafán-Vidales, C.A. Arancibia-Bulnes, V.H. Ramos-Sánchez, A.K. Cuentas-Gallegos, A sustainable approach to produce activated carbons from pecan nutshell waste for environmentally friendly supercapacitors, Carbon N. Y. 148 (2019) 403–412, https://doi.org/10.1016/j.carbon.2019.04.017.
[33] K. Kumar, R.K. Saxena, R. Kothari, D.K. Suri, N.K. Kaushik, J.N. Bohra, Correlation between adsorption and x-ray diffraction studies on viscose rayon based activated carbon cloth, Carbon N. Y. 35 (1997) 1842–1844, https://doi.org/10.1016/S0008-6223(97)87258-2.
[34] A.K. Samanta, G. Basu, L. Mishra, Role of major constituents of coconut fibres on absorption of ionic dyes, Ind. Crops Prod. 117 (2018) 20–27, https://doi.org/10.1016/j.indcrop.2018.02.080.
[35] J. Andas, P. Joseph, Synthesis and characterization of low cost activated carbon from dried rind Garcinia xanthochymus, AIP Conference Proceedings 2332 (2021), https://doi.org/10.1063/5.0042908.
[36] Y.J. Zhang, Z.J. Xing, Z.K. Duan, M. Li, Y. Wang, Effects of steam activation on the pore structure and surface chemistry of activated carbon derived from bamboo waste, Appl. Surf. Sci. 315 (2014) 279–286, https://doi.org/10.1016/j.apsusc.2014.07.126.
[37] M. Changmai, P. Banerjee, K. Nahar, M.K. Purkait, A novel adsorbent from carrot, tomato and polyethylene terephthalate waste as a potential adsorbent for Co (II) from aqueous solution: Kinetic and equilibrium studies, J. Environ. Chem. Eng. 6 (2018) 246–257, https://doi.org/10.1016/j.jece.2017.12.009.
[38] J. Yang, Y. Wang, J. Luo, L. Chen, Highly nitrogen-doped graphitic carbon fibers from sustainable plant protein for supercapacitor, Ind. Crops Prod. 121 (2018) 226–235, https://doi.org/10.1016/j.indcrop.2018.05.013.
[39] A. Gopalakrishnan, S. Badhulika, Effect of self-doped heteroatoms on the performance of biomass-derived carbon for supercapacitor applications, J. Power Sources. 480 (2020), https://doi.org/10.1016/j.jpowsour.2020.228830.
[40] F. Liu, Z. Wang, H. Zhang, L. Jin, X. Chu, B. Gu, H. Huang, W. Yang, Nitrogen, oxygen and sulfur co-doped hierarchical porous carbons toward high-performance supercapacitors by direct pyrolysis of kraft lignin, Carbon N. Y. 149 (2019) 105–116, https://doi.org/10.1016/j.carbon.2019.04.023.
[41] H. Xu, Y. Zhang, L. Wang, Y. Chen, S. Gao, Hierarchical porous biomass-derived carbon framework with ultrahigh surface area for outstanding capacitance supercapacitor, Renew. Energy. 179 (2021) 1826–1835, https://doi.org/10.1016/j.renene.2021.08.008.
[42] C. Ding, T. Liu, X. Yan, L. Huang, S. Ryu, J. Lan, Y. Yu, W.H. Zhong, X. Yang, AN Ultra-microporous carbon material boosting integrated capacitance for cellulose-based supercapacitors, Nano-Micro Lett. 12 (2020) 63, https://doi.org/10.1007/s40820-020-0393-7.
[43] Y. Wang, M. Qiao, X. Mamat, Nitrogen-doped macro-meso-micro hierarchical ordered porous carbon derived from ZIF-8 for boosting supercapacitor performance, Appl. Surf. Sci. 540 (2021), https://doi.org/10.1016/j.apsusc.2020.148352.
[44] M.D. Liao, C. Peng, S.P. Hou, J. Chen, X.G. Zeng, H.L. Wang, J.H. Lin, Large-Scale Synthesis of Nitrogen-Doped Activated Carbon Fibers with High Specific Surface Area for High-Performance Supercapacitors, Energy Technol. 8 (2020) 1901477, https://doi.org/10.1002/ente.201901477.
[45] S.S. Sekhon, J.S. Park, Biomass-derived N-doped porous carbon nanosheets for energy technologies, Chem. Eng. J. 425 (2021), https://doi.org/10.1016/j.cej.2021.129017.
[46] F. Zhang, T. Zhang, X. Yang, L. Zhang, K. Leng, Y. Huang, Y. Chen, A high-performance supercapacitor-battery hybrid energy storage device based on graphene-enhanced electrode materials with ultrahigh energy density, Energy Environ. Sci. 6 (2013) 1623–1632, https://doi.org/10.1039/c3ee40509e.
[47] Y. Cai, Y. Luo, H. Dong, X. Zhao, Y. Xiao, Y. Liang, H. Hu, Y. Liu, M. Zheng, Hierarchically porous carbon nanosheets derived from Moringa oleifera stems as electrode material for high-performance electric double-layer capacitors, J. Power Sources. 353 (2017) 260–269, https://doi.org/10.1016/j.jpowsour.2017.04.021.
[48] K. Aruchamy, K. Dharmalingam, C.W. Lee, D. Mondal, N. Sanna Kotrappanavar, Creating ultrahigh surface area functional carbon from biomass for high performance supercapacitor and facile removal of emerging pollutants, Chem. Eng. J. 427 (2022), https://doi.org/10.1016/j.cej.2021.131477.
[49] Y. Wang, Z. Zhao, W. Song, Z. Wang, X. Wu, From biological waste to honeycomb-like porous carbon for high energy density supercapacitor, J. Mater. Sci. 54 (2019) 4917–4927, https://doi.org/10.1007/s10853-018-03215-8.